Nuclear Inst. and Methods in Physics Research, A 1048 (2023) 167952

Contents lists available at ScienceDirect

Nuclear Inst. and Methods in Physics Research, A

journal homepage: www.elsevier.com/locate/nima

The 100μPET project: A small-animal PET scanner for ultra-high resolution molecular imaging with monolithic silicon pixel detectors

Franck Cadoux [a], Roberto Cardella [a], Giuseppe Iacobucci [a], Luca Iodice [a], Didier Ferrere [a], Sergio Gonzalez-Sevilla [a], Thanushan Kugathasan [a], Fulvio Martinelli [a], Lorenzo Paolozzi [a,b], Antonio Picardi [a], Jihad Saidi [a], Mateus Vicente [a,*], Stefano Zambito [a]

[a] Geneva University, Switzerland
[b] CERN, Switzerland

ARTICLE INFO

Keywords:
Positron
Emission
Tomography
Monolithic
Silicon sensor
Pixel detector
Ultra-high resolution
Molecular imaging

ABSTRACT

Recent developments in semiconductor pixel detectors allow a new generation of positron-emission tomography (PET) scanners that, combined with advanced image reconstruction algorithms, will allow for a few hundred microns spatial resolutions. Such novel scanners will pioneer ultra-high resolution molecular imaging, a field that is expected to have an enormous impact in several medical domains, neurology among others.

The University of Geneva, the École Polytechnique Fédérale de Lausanne, and the University of Lucerne, have launched the 100μPET project that aims to produce a small-animal PET scanner with ultra-high resolution. The scanner will be composed of 4 "towers", each containing a stack of 60 monolithic silicon pixel sensors for the direct measurement of the annihilation photons. The sensors are 270 μm thick, providing unprecedented depth-of-interaction measurement. Monte Carlo simulations were done simulating different scanner conditions, resulting in a spatial resolution down to 0.2 mm FWHM and a sensitivity of 3.2%.

1. Introduction

The 100μPET project aims at the construction of a novel generation small-animal Positron Emission Tomography (PET) scanner, with unprecedented volumetric spatial resolution to perform ultra-high resolution molecular imaging of the onset and progression of atherosclerosis in Atherosclerosis-prone apolipoprotein E-deficient (ApoE-/-) mice [1].

PET is the most sensitive imaging technique to register molecular interactions of specific bio-markers, biochemicals and pharmaceuticals, in an organism. The sensitivity to track these bio-markers, to their lowest concentrations, is achieved by the addition of specific positron-emitting radionuclides, which can be attached to the specific bio-markers without disturbing their biological function [2]. These radio-labeled bio-markers can then be traced by the detection of the photons coming from the positron annihilation. PET imaging relies in detecting the two photons from the electron–positron annihilation, and reconstruct in a 3D space the vertex position of the annihilation.

The advent of PET imaging has led to a deeper understanding of the development, progression, and treatment response for a variety of major diseases, such as cardiovascular diseases, neurodegeneration, and malignant neoplasms. While the advantage of PET is its unprecedented sensitivity to detect low molecular masses of the radiotracer, its weakness is its low resolution to image sub-millimeter features [3].

2. Spatial resolution

Spatial Resolution (SR) is an important metric for quantifying the imaging performance while characterizing PET systems, indicating the smallest volume of a structure that can be reconstructed with accuracy. The most fundamental limit of SR in PET imaging is determined by the physics of the positron annihilation. After the radiotracer positron emission, the positron will travel a random path before annihilation. Upon annihilation, the positron will have some remaining momentum, resulting in an small angular deviation from the 180° photons' back-to-back angle, known as acolinearity effect. In addition to this fundamental limit, PET SR depends also on the scanner design, which can be optimized, and the following photons scattering within the scanner, which can be modeled and filtered out in the imaging reconstruction.

High SR is typically pursued by: improvements in the scintillating crystal and its respective coupling to a photodetector; in the detector's signal processing electronics; data modeling and analysis; and imaging reconstruction algorithms. Depth-Of-Interaction (DOI) measurement capability is one of the most important improvements in new generations of high-resolution PET detectors. Accurate DOI information is used to provide an uniform SR across the scanner's field-of-view, an effect known as parallax. Various DOI encoding systems have been

* Corresponding author.
E-mail address: mvicente@unige.ch (M. Vicente).

https://doi.org/10.1016/j.nima.2022.167952
Received 29 July 2022; Received in revised form 2 December 2022; Accepted 3 December 2022
Available online 19 December 2022

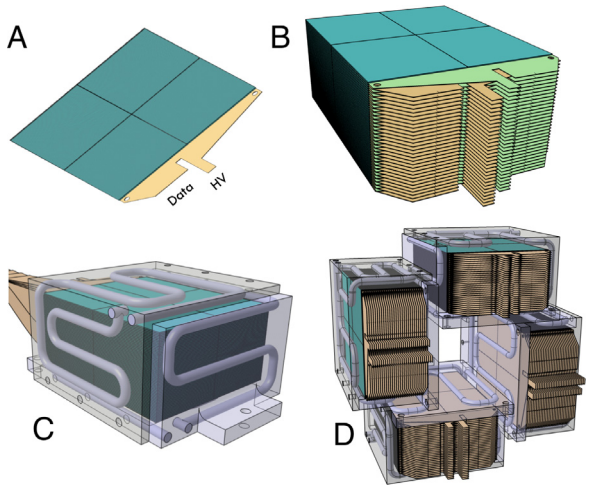

Fig. 1. (A) 4 pixel detectors (in blue) coupled to a read-out FPC (yellow). (B) Stack of 60 detection layers. (C) Stack inside cooling block. (D) 4 towers assembly.

developed [3], and the resolutions achieved today are in the order of 1 to 5 mm^3, with scanner sensitivities between 2 and 10% [4].

3. PET with semiconductor detectors

Ultra-high resolution will be achieved by replacing the standard scintillating crystals and its following front-end read-out system, achieving typical sensor's volumetric granularity of $4 \times 4 \times 20$ mm^3, with a multi-layer stack of CMOS imaging sensors, based on silicon pixel detectors used in high energy physics experiments, following a trend already in place in other fields [5]. In CMOS pixel detectors, the same silicon substrate is used as sensor media and for the CMOS signal processing and read-out circuits, creating a direct detection channel with integrated read-out. A 270 μm thick ASIC containing a pixel matrix with ≈60 000 channels, with a pitch of 100 μm, will be stacked 60 times, with circuit and glue layers in between summing up to 400 μm thick detection layers, resulting on a scanner granularity of 0.004 mm^3. 4 stacks will be placed around the investigated subject. Fig. 1 illustrates a possible scanner assembly.

In this design, each pixel in the layered detectors is a ultra-small direct detection 3D channel that can be readout unambiguously. The presence of a detecting layer every 400 μm provides an outstanding DOI measurement, ensuring that the SR will not degrade away from the center of the scanner, making it free of parallax distortion. These developments in instrumentation will allow to overcome the current resolution limit of PET scanners, bringing the SR closer to the physical intrinsic limitation given by the 100 μm mean free path of the FDG positrons in biological tissues [6].

PET scanners made by semiconductor layers with direct detection have been attempted in the past, [7]. The complexity and the high cost of the hybrid silicon sensors available at the time, however, has been an insurmountable limiting factor. Today, the availability of monolithic silicon pixel sensors re-opens the possibility of using semiconductor detector to build multi-layered scanners, allowing for the quantum leap needed to open the field to ultra-high resolution molecular imaging

4. Past developments

The small-animal 100μPET scanner is an evolution of our previous TT-PET (Thin-Time-Of-Flight PET) project [8]. A silicon-based multi-layered scanner, it had a cylindrical geometry with 16 wedge-shaped stacks with 60 layers of 50 μm thick lead absorber layers interleaved with 100 μm thick silicon pixel detectors, with 500 μm pixel pitch, and time resolution down to 110 ps. Each of the 16 stacks required its own cooling system, summing up to approximately 25% of the scanner's volume, reducing the two-photon coincidence sensitivity by about 56%. For this reason, a simplified square geometry with minimum cooling in the active detection volume was chosen for the 100μPET scanner.

After the TT-PET project, we proved to be able to operate our electronics at a power consumption 30 times smaller, while still achieving an outstanding 200 ps time resolution [9]. This allows us to propose an even more performant small-animal PET scanner, having pixel sizes possibly as small as 100×100 μm^2.

5. Monte Carlo simulation

Monte Carlo simulations are used for exploring the resolution limits and predicting the performance of different scanner designs, being possible to quantify how much each design choice cost in view of scanner's SR and sensitivity.

A simulation was set-up using the Allpix2 framework [10]. The framework is based on the Geant4 framework to simulate the processes involved in the positron emission and annihilation in matter, photons propagation and scattering through the scanner, and the energy deposition in the detector by the electrons from the converted photons. The energy spectrum of the positron source follows a Rayleigh distribution with most probable value of 200 keV and cut-off at 635 keV [6], including the positron range and photons acolinearity in the simulation.

With the energy deposited by the electron, electron–holes pair are created (one for each 3.6 eV deposited) and they are transported via drift and diffusion towards the simulated pixel's electrodes for collection. A signal threshold of about 2700 electrons (equivalent to an energy deposition of 10 keV) is applied to have a given pixel with a hit recorded.

The simulated geometry is shown in Fig. 2. 60 layers of a monolithic silicon pixel detectors and their Kapton-based read-out flexible circuit are stacked and placed inside an aluminium cooling block with 3 mm thick walls. 4 of such stacks surrounds the patient bed. One variant geometry was simulated, where 50 μm layers of Bismuth (an absorber material with higher atomic number, with respect to the silicon detection layers, to increase the number of photons converted) are included on each of the 60 detection layers, intended to increase the scanner's sensitivity. The scanner's cubic cavity is filled with an uniform water-phantom for simulating possible scattering.

As recommended by the National Electrical Manufacturers Association (NEMA) standards for both clinical and small animal PET systems, a point-like positron source is simulated at the center of the scanner, and then it is displaced towards a detection tower in 5 mm steps.

160 millions events were simulated, with a single positron annihilation per event. In this way, no timing is considered in this simulation. As quality criteria for the construction of the Line-of-Response (LoR) we only select events in which two hit clusters are detected, each on a different scanner's tower. Doing so we filter out events with multiple (>2) photons interactions above detection threshold, generating ambiguous LORs, while preserving possible random coincidences. The 3D position of each of the two hit clusters is used as an end-point of the LoR, and the number of LoR detected is considered as the scanner's sensitivity. Moreover, because how photons are detected when using the thin silicon sensors, no energy discrimination is used and all, unambiguous, interacting events are used [11].

6. Scanner performance results

While NEMA 2008-4 proposes SR to be measured by reconstructing point source scans using the filtered back-projection algorithm and calculating the Full Width at Half Maximum (FWHM) and at Tenth Maximum (FWTM) from the profiles along the radial and tangential directions, here our FWHM is calculated from the distribution of distances between the point of closest approach in the LoR to the point of positron emission (0,0,0), accounting in this way the intrinsic uncertainty given by the random positron range after its emission.

Table 1
Spatial resolution and sensitivity measured, for different scanner's geometries.

Geometry	Pixel pitch [mm]	Spatial resolution [mm]		LoR sensitivity [%]		
		FWHM	FWTM	Up to 0.2 mm	Up to 0.5 mm	Up to 20 mm
Without absorber	0.1	$0.264^{+0.004}_{-0.004}$	$0.977^{+0.033}_{-0.028}$	0.55	1.04	3.29
	0.2	$0.287^{+0.006}_{-0.006}$	$1.04^{+0.04}_{-0.04}$	0.56	1.06	3.34
With absorber	0.1	$0.326^{+0.006}_{-0.0046}$	$1.23^{+0.04}_{-0.05}$	0.87	1.77	4.81

Table 2
Spatial resolution as function of source position.

Displacement [mm]	SR in LOR plane (Without absorber)				SR in LOR plane (With absorber)			
	Y coord. [mm]		Z coord. [mm]		Y coord. [mm]		Z coord. [mm]	
	FWHM	FWTM	FWHM	FWTM	FWHM	FWTM	FWHM	FWTM
0	$0.266^{+0.004}_{-0.004}$	$0.984^{+0.036}_{-0.03}$	$0.264^{+0.004}_{-0.004}$	$0.977^{+0.033}_{-0.028}$	$0.347^{+0.016}_{-0.015}$	$1.15^{+0.09}_{-0.07}$	$0.326^{+0.006}_{-0.0046}$	$1.23^{+0.04}_{-0.05}$
5	$0.267^{+0.004}_{-0.004}$	$0.995^{+0.035}_{-0.028}$	$0.265^{+0.004}_{-0.003}$	$0.986^{+0.024}_{-0.023}$	$0.348^{+0.017}_{-0.017}$	$1.16^{+0.09}_{-0.08}$	$0.352^{+0.03}_{-0.03}$	$1.16^{+0.01}_{-0.02}$
10	$0.269^{+0.004}_{-0.004}$	$1.01^{+0.03}_{-0.024}$	$0.273^{+0.004}_{-0.004}$	$1.02^{+0.030}_{-0.031}$	$0.332^{+0.006}_{-0.005}$	$1.27^{+0.04}_{-0.04}$	$0.335^{+0.007}_{-0.007}$	$1.27^{+0.05}_{-0.05}$
15	$0.278^{+0.004}_{-0.003}$	$1.07^{+0.02}_{-0.03}$	$0.286^{+0.005}_{-0.005}$	$1.08^{+0.04}_{-0.03}$	$0.340^{+0.005}_{-0.006}$	$1.32^{+0.04}_{-0.05}$	$0.352^{+0.010}_{-0.011}$	$1.35^{+0.09}_{-0.08}$

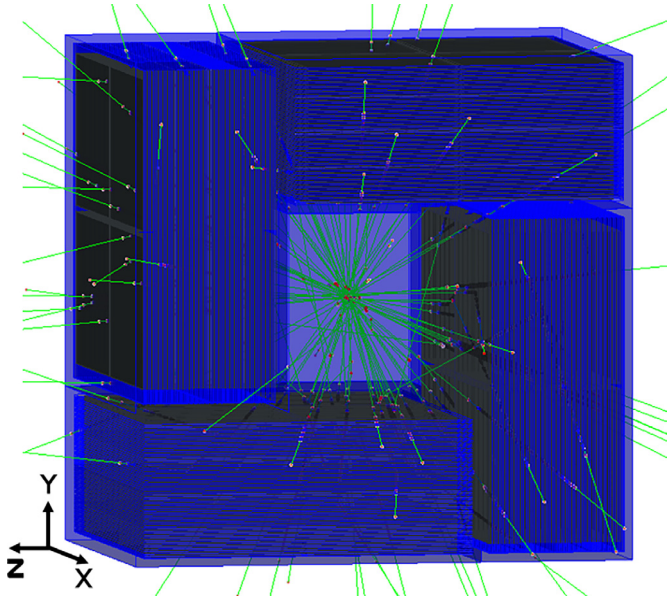

Fig. 2. Simulated geometry, with 4 detection towers, each with 60 layers of pixel detectors ASICs, and a positron source with ≈ 100 annihilations.

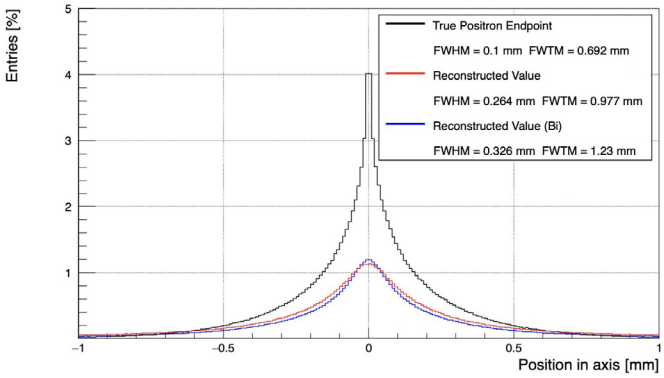

Fig. 3. Simulated spatial resolution for the scanner with and without the absorber layers, compared with the simulated positron range.

To account for the uncertainty of the annihilation point along the reconstructed LoR, the distance of closest approach of the LoR to the positron source is measured in the 2D plane transversal to the LoR, decomposed in the plane's coordinate axes. As such transversal plane and coordinate axes are unique for each LoR constructed, all LoR are rotated towards the X axis (our scanner axis), making all LoR perpendicular planes being parallel to the global YZ. Therefore our LoR-source distance is measured in the global Y and Z axis. This alternative figure-of-merit provides a physical measurement of the resolution, without being impacted by the reconstruction technique used.

The unprecedented sensor and read-out voxel size of such scanner results in a point-spread function FWHM of 0.264 mm, shown in Fig. 3 and detailed in Table 1, proving ground-breaking SR. This resolution put us closer to the fundamental limit given by the uncertainty of the positron random trajectory after emission, also visible in Fig. 3 for comparison. This FWHM is expected to be improved when using advanced imaging reconstruction techniques.

The simulation was repeated with 200 μm pixel pitch and we see that this results in a marginal effect in the SR, shown in Table 1. In contrast to assigning the photon's interaction position to the center of a given pixel if the photon's signal is detected by a single pixel, a better positioning accuracy is achieved when signals from multiple pixels are detected, generating a pixel cluster for which a centroid position can be calculated. As expected, with the 200 μm pixel size we see 14% more single-pixel clusters, hence worsening slightly the SR. This means that the scanner can be operated without significant SR deterioration with 1/4th of the channels and power consumption, or keeping the same power and allowing more elaborated signal processing electronics, pushing the time resolution for example.

It is possible to quantify the sensitivity of the scanner as function of the absolute 3D distance from the LoR to the positron source. A sensitivity of up to 3.29% is measured for the scanner without the absorber layers. When the high Z material layers are included in the scanner, the sensitivity increases by about 50%, reaching 4.8%, while deteriorating the FWHM from 0.264 mm to 0.326 mm.

The same positron source was also simulated at (0, 5 mm, 0), (0, 10 mm, 0) and (0, 15 mm, 0). The FWHM and FWTM were evaluated for each point as mentioned above. The results are presented in Table 2, showing a FWHM below or equal 0.28 mm in all directions, without the absorber layer, and 0.34 mm with the absorber layers included.

7. Conclusions

The introduction of our method of multi-layer monolithic silicon pixel PET scanners will avoid many of the image-degrading effects in current PET systems caused by the physics of crystal photon detectors, e.g.: the very precise DOI granularity of 400 μm of our scanner architecture provides constant image resolution away from the center of the transversal and axial FOV, making it free of parallax error. Moreover, the unique voxel size achieved provides an excellent spatial resolution of 0.26 mm FWHM.

This will open the horizon to the utilization of the semiconductor sensor technology and related integrated electronics developed for particle physics and commercial applications. Such a new generation instrument will allow to overcome the key weakness of molecular imaging with PET.

An example of future important developments, which stems from the research activity of the UNIGE-DPNC group, is offered by the possibility to instrument a silicon-sensor like that of this project with a gain layer, therefore allowing for a much better time resolution than the 200 ps proposed here. At present, we obtained the world's best time resolution of 36 ps for ionizing radiation with pixelated silicon without internal gain mechanism [12]. As demonstrated by our patent [13] and presently under development within the H2020 ERC Advanced grant MONOLITH [14], the addition of a gain layer to our detector ASIC is expected to provide picosecond-level time resolution. Utilization of these extreme time resolutions in future PET scanners will allow for real-time PET imaging, which could enable not only extremely detailed time-progression studies, but also enable improved real-time PET-guided biopsies, and improved real-time PET-guided therapies.

Successful completion of the proposed project will provide the pioneering of ultra-high resolution molecular imaging (below 250 μm) and its demonstration in the study of disease progression and treatment monitoring in animal models.

Declaration of competing interest

The authors declare that they have no known competing financial interests or personal relationships that could have appeared to influence the work reported in this paper.

Acknowledgement

This research is supported by the Swiss National Science Foundation SINERGIA grant CRSII5_198569.

References

[1] G. Iacobucci, M. Unser, M. Walter, The 100μPET project: Pioneering ultra-high resolution molecular imaging, 2022, https://p3.snf.ch/Project-198569, accessed: 2022-06-27.

[2] T.L. Jones, D.W. Townsend, History and future technical innovation in positron emission tomography, J. Med. Imaging (Bellingham Wash.) 4 (1) (2017) 011013, http://dx.doi.org/10.1117/1.jmi.4.1.011013.

[3] I. Mohammadi, I.F.C. Castro, P.M.M. Correia, A.L.M. Silva, J.F.C.A. Veloso, Minimization of parallax error in positron emission tomography using depth of interaction capable detectors: methods and apparatus, Biomed. Phys. Eng. Express 5 (6) (2019) 062001, http://dx.doi.org/10.1088/2057-1976/ab4a1b.

[4] B. Weissler, Digital PET/MRI for Preclinical Applications (Dissertation), RWTH Aachen, Aachen, 2016, Dissertation, RWTH Aachen, 2016.

[5] J. Jakůbek, Semiconductor Pixel detectors and their applications in life sciences, J. Instrum. 4 (03) (2009) P03013, http://dx.doi.org/10.1088/1748-0221/4/03/p03013.

[6] C.S. Levin, E.J. Hoffman, Calculation of positron range and its effect on the fundamental limit of positron emission tomography system spatial resolution, Phys. Med. Biol. 44 (3) (1999) 781–799, http://dx.doi.org/10.1088/0031-9155/44/3/019.

[7] M. Chmeissani, M. Kolstein, J.G. Macias-Montero, C. Puigdengoles, J. García, X. Prats, R. Martínez, First results of a highly granulated 3D CdTe detector module for PET, Phys. Med. Biol. 63 (2) (2018) 025032, http://dx.doi.org/10.1088/1361-6560/aaa44c.

[8] G. Iacobucci, O. Ratib, M. Weber, TT-PET: Thin Time-of-Flight PET with depth of interaction measurement capability based on very-low noise Silicon-Germanium BJT electronics and semiconductor detector, 2022, http://p3.snf.ch/Project-160808, accessed: 2022-06-27.

[9] L. Paolozzi, R. Cardarelli, S. Débieux, Y. Favre, D. Ferrère, S. Gonzalez-Sevilla, G. Iacobucci, M. Kaynak, F. Martinelli, M. Nessi, H. Rücker, I. Sanna, D. Sultan, P. Valerio, E. Zaffaroni, Time resolution and power consumption of a monolithic silicon pixel prototype in SiGe BiCMOS technology, J. Instrum. 15 (11) (2020) P11025, http://dx.doi.org/10.1088/1748-0221/15/11/p11025.

[10] S. Spannagel, K. Wolters, D. Hynds, N. Alipour Tehrani, M. Benoit, D. Dannheim, N. Gauvin, A. Nürnberg, P. Schütze, M. Vicente, Allpix2: A modular simulation framework for silicon detectors, Nucl. Instrum. Methods Phys. Res. A 901 (2018) 164–172, http://dx.doi.org/10.1016/j.nima.2018.06.020.

[11] J.R. Stickel, S.R. Cherry, High-resolution PET detector design: modelling components of intrinsic spatial resolution, Phys. Med. Biol. 50 (2) (2004) 179, http://dx.doi.org/10.1088/0031-9155/50/2/001.

[12] G. Iacobucci, L. Paolozzi, P. Valerio, T. Moretti, F. Cadoux, R. Cardarelli, R. Cardella, S. Débieux, Y. Favre, D. Ferrere, S. Gonzalez-Sevilla, Y. Gurimskaya, R. Kotitsa, C. Magliocca, F. Martinelli, M. Milanesio, M. Münker, M. Nessi, A. Picardi, J. Saidi, H. Rücker, M.V.B. Pinto, S. Zambito, Efficiency and time resolution of monolithic silicon pixel detectors in SiGe BiCMOS technology, J. Instrum. 17 (02) (2022) P02019, http://dx.doi.org/10.1088/1748-0221/17/02/p02019.

[13] G. Iacobucci, L. Paolozzi, P. Valerio, Multi-junction pico-avalanche detector, 2018, Europe Patent 18 207 008.6.

[14] G. Iacobucci, MONOLITH - Monolithic Multi-Junction Picosecond Avalanche Detector for future physics experiments and applications, 2020, H2020 ERC Advanced grant Agreement No. 884447.